Assault frequency and preformation probability of the α emission process

H. F. Zhang
School of Nuclear Science and Technology, Lanzhou University, Lanzhou 730000, People's Republic of China

G. Royer
Laboratoire Subatech, UMR 6457, IN2P3/CNRS-Université-Ecole des Mines, Nantes, France

J. Q. Li
Institute of Modern Physics, Chinese Academy of Sciences, Lanzhou 730000, People's Republic of China

(Received 13 May 2011; revised manuscript received 5 July 2011; published 19 August 2011)

A study of the assault frequency and preformation factor of the α-decay description is performed from the experimental α-decay constant and the penetration probabilities calculated from the generalized liquid-drop model (GLDM) potential barriers. To determine the assault frequency a quantum-mechanical method using a harmonic oscillator is introduced and leads to values of around 10^{21} s^{-1}, similar to the ones calculated within the classical method. The preformation probability is around 10^{-1}–10^{-2}. The results for even-even Po isotopes are discussed for illustration. While the assault frequency presents only a shallow minimum in the vicinity of the magic neutron number 126, the preformation factor and mainly the penetrability probability diminish strongly around $N = 126$.

DOI: 10.1103/PhysRevC.84.027303 PACS number(s): 23.60.+e, 21.10.Jx, 21.60.Ev

The α-decay theory was developed in 1928 [1,2]. It describes the α radioactivity as a quantum tunneling through the potential barrier separating the mother nucleus energy and the total energy of the separated α particle and daughter nucleus. Later on, cluster-like [3–8] and fission-like [9–14] theories were used to explain the α emission process. The decay constant λ is the product of three terms: the assault frequency ν, the barrier penetrability P, and the α preformation probability P_α. Often, the assault frequency is calculated supposing that the α particle moves classically back and forth inside the nucleus and is even sometimes taken as a constant. The cluster preformation probability corresponds to the penetrability of the part of the barrier before reaching the separation point, while the barrier penetrability is associated with the external part of the barrier when the fragments are separated.

First, the potential barrier governing the α-particle emission has been determined within the generalized liquid-drop model (GLDM), taking into account the mass and charge asymmetry [10,14,15]. The total energy is the sum of the volume, surface, Coulomb, and proximity energies. When the nuclei are separated,

$$E_V = -15.494\left[\left(1 - 1.8I_1^2\right)A_1 + \left(1 - 1.8I_2^2\right)A_2\right] \text{ MeV}, \quad (1)$$

$$E_S = 17.9439\left[\left(1 - 2.6I_1^2\right)A_1^{2/3} + \left(1 - 2.6I_2^2\right)A_2^{2/3}\right] \text{ MeV}, \quad (2)$$

$$E_C = 0.6e^2Z_1^2/R_1 + 0.6e^2Z_2^2/R_2 + e^2Z_1Z_2/r, \quad (3)$$

where A_i, Z_i, R_i, and I_i are the mass numbers, charge numbers, radii, and relative neutron excesses of the two nuclei, respectively; r is the distance between the mass centers.

For one-body shapes, the surface and Coulomb energies are defined as

$$E_S = 17.9439(1 - 2.6I^2)A^{2/3}\left(S/4\pi R_0^2\right) \text{ MeV}, \quad (4)$$

$$E_C = 0.6e^2(Z^2/R_0) \times 0.5 \int [V(\theta)/V_0][R(\theta)/R_0]^3 \sin\theta d\theta. \quad (5)$$

S is the surface of the one-body deformed nucleus. $V(\theta)$ is the electrostatic potential at the surface, and V_0 is the surface potential of the sphere.

When there are nucleons in regard in a neck or a gap between separated fragments, a proximity energy must be added to take into account the effects of the nuclear forces between the close surfaces,

$$E_{\text{Prox}}(r) = 2\gamma \int_{h_{\min}}^{h_{\max}} \Phi\left[D(r,h)/b\right] 2\pi h dh, \quad (6)$$

where h is the distance varying from the neck radius or zero to the height of the neck border. D is the distance between the surfaces in regard, and $b = 0.99$ fm is the surface width. Φ is the proximity function. The surface parameter γ is the geometric mean between the surface parameters of the two fragments. This term is essential to describe smoothly the one-body to two-body transition and to obtain reasonable potential barrier heights. It moves the barrier top to an external position and strongly decreases the pure Coulomb barrier. The experimental Q_α is taken into account. It has been previously shown that the combination of this GLDM and of a quasimolecular shape sequence allows us to reproduce the fusion barrier heights and radii, the fission, the α decay, and the proton and cluster radioactivity data [10,15–18].

The barrier penetrability P has been calculated within the action integral:

$$P = \exp\left[-\frac{2}{\hbar}\int_{R_{\text{in}}}^{R_{\text{out}}} \sqrt{2B_{(r)}(E_{(r)} - E_{(\text{sphere})})}\, dr\right]. \quad (7)$$

Then the knowledge of the experimental decay constant λ and of the calculated barrier penetrability P allows us to determine

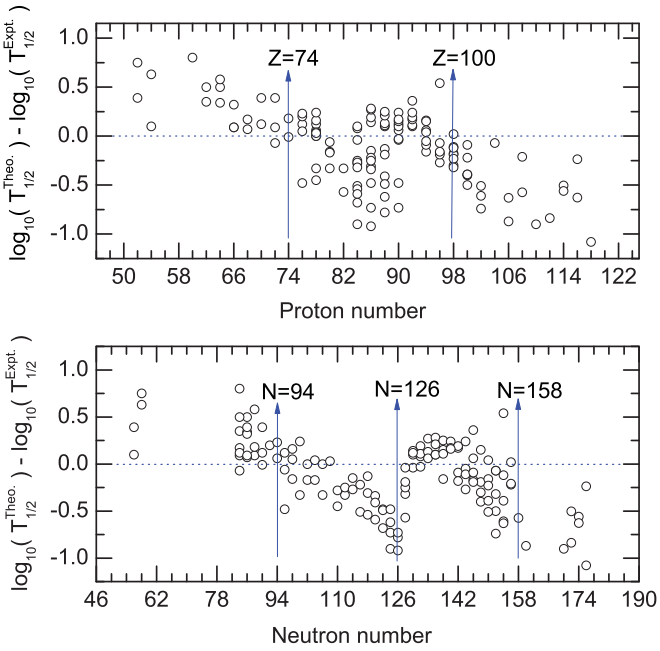

FIG. 1. (Color online) The top panel (bottom panel) shows the deviations between calculated [10] and experimental α-decay half-lives for 131 even-even nuclei as a function of the proton number (neutron number).

the behavior of the product $P_\alpha \nu$ via the relation

$$\lambda = P_\alpha \nu P. \tag{8}$$

Let us first recall that in a previous study [10] the ratio λ/P was fixed as 10^{20} s^{-1}. In Fig. 1, the deviation between the values of $\log_{10}[T_{1/2}\,(\mathrm{s})]$ within this approximation and the experimental ones is shown as a function of proton number (top panel) and neutron number (bottom panel). For the subset of the 131 even-even nuclei the root-mean-square deviation is 0.35. The theoretical data are slightly higher than the experimental ones for the lighter nuclei and systematically lower for the heaviest systems. When the proton number is under 74 (top panel) or the neutron number is under 94 (bottom panel), the calculations are higher than the experimental data, but for nuclei where the proton number is beyond 100 or the neutron number is beyond 158, these theoretical predictions are lower than the experimental data. In addition, the deviations are larger when the proton number is about 82 and the neutron number is about 126. Some details on nuclear structure are missing when a fixed ratio λ/P is assumed.

In the present work, the empirical values of λ/P are extracted for 154 even-even nuclei. The experimental α-decay half-lives are given in Refs. [19–22]. Figure 2 displays a plot of $\log_{10}\lambda/P$ as a function of the neutron number. The values present a sharp decrease around the neutron magic number $N = 126$, reconfirming this neutron-closure shell structure. For a neutron number beyond about 155, the decreased trend appears again, giving us some signals for an island of stability of superheavy nuclei. So this ratio is in reality slightly sensitive to the nuclear structure and can at least be used to detect shell effects.

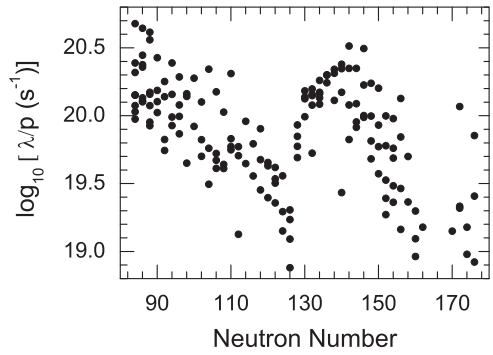

FIG. 2. $\log_{10}(\lambda/P)$ for 154 even-even nuclei vs the neutron number.

As an example the extracted λ/P values are shown in the sixth column of the Table I for even-even Po isotopes. The range spans from 10^{19} s^{-1} to more than 10^{20} s^{-1}.

One way to determine the assault frequency is to imagine the α particle moving back and forth classically inside the nucleus with a velocity $v = \sqrt{\frac{2E_\alpha}{M}}$. Then it presents itself at the barrier with a frequency

$$\nu_C = \left(\frac{1}{2R}\sqrt{\frac{2E_\alpha}{M}}\right), \tag{9}$$

where R is the radius of the parent nucleus, E_α is the kinetic energy of the α particle, corrected for recoil, and M is its mass. Then the preformation factor P_α of an α cluster inside the mother nucleus can be estimated using Eq. (8).

As an example, the calculated assault frequency ν from Eq. (9) as well as the preformation factor deduced from Eq. (8) and from the experimental constant decay are shown in the seventh and ninth columns of Table I, respectively, for the Po isotopes. The order of magnitude of ν is 10^{21} s^{-1}. Consequently, the preformation probability is of the order of 10^{-2}–10^{-1}. Both the penetration and preformation probabilities are reduced in the vicinity of the magic neutron number 126, but the penetration probability range is very large compared to that of the preformation factor. The penetration probability, which is strongly connected to the Q_α value, determines mainly the α-decay half-life.

An approach to deal with the assault frequency is proposed within a microscopic method deriving from the viewpoint of quantum mechanics. It assumes that the α particle that will be emitted vibrates near the surface of the parent nucleus in a harmonic oscillator potential $V(r) = -V_0 + \frac{1}{2}\mu\omega^2 r^2$ with classical frequency ω and reduced mass μ. The virial theorem leads to

$$\mu\omega^2\overline{r^2} = \left(2n_r + \ell + \tfrac{3}{2}\right)\hbar\omega, \tag{10}$$

where n_r and ℓ are the radial quantum number (corresponding to number of nodes) and angular momentum quantum number, respectively. $\sqrt{\overline{r^2}} = \langle\psi|r^2|\psi\rangle^{1/2}$ is the rms radius of outermost α distributions in quantum mechanics. It equals the rms radius R_n of the parent nucleus. The assault frequency ν_M is related

TABLE I. Characteristics of the α decay for the even-even Po isotopes. The first four columns correspond to the mother nucleus, the experimental Q_α, $\log_{10}[T_{1/2}\ (\mathrm{s})]$, and the experimental decay constant λ, respectively. The fifth column is the penetration probability. The sixth through eighth columns give the ratio λ/P, the assault frequency obtained within the classical approach, and the assault frequency using a quantum-mechanical approach, respectively. The last column displays the preformation probability.

Nuclei	Q_α (MeV)	$\log_{10}[T_\alpha\ (\mathrm{s})]$	$\lambda\ (\mathrm{s}^{-1})$	P	$\lambda/P\ (\mathrm{s}^{-1})$	$\nu_C\ (\mathrm{s}^{-1})$	$\nu_M\ (\mathrm{s}^{-1})$	P_α
$^{188}_{84}$Po	8.087	−3.40	1.733×10^{3}	8.129×10^{-17}	2.133×10^{19}	1.451×10^{21}	2.055×10^{21}	0.0147
$^{190}_{84}$Po	7.693	−2.60	2.772×10^{2}	5.907×10^{-18}	4.698×10^{19}	1.411×10^{21}	2.039×10^{21}	0.0333
$^{192}_{84}$Po	7.319	−1.54	2.392×10^{1}	3.909×10^{-19}	6.119×10^{19}	1.371×10^{21}	2.023×10^{21}	0.0446
$^{194}_{84}$Po	6.990	−0.41	1.782×10^{0}	3.249×10^{-20}	5.485×10^{19}	1.335×10^{21}	2.008×10^{21}	0.0410
$^{196}_{84}$Po	6.660	0.76	1.205×10^{-1}	2.041×10^{-21}	5.904×10^{19}	1.299×10^{21}	1.993×10^{21}	0.0455
$^{198}_{84}$Po	6.310	2.18	4.580×10^{-3}	8.283×10^{-23}	5.529×10^{19}	1.259×10^{21}	1.978×10^{21}	0.0439
$^{200}_{84}$Po	5.980	3.79	1.124×10^{-4}	3.066×10^{-24}	3.666×10^{19}	1.222×10^{21}	1.963×10^{21}	0.0300
$^{202}_{84}$Po	5.700	5.13	5.138×10^{-6}	1.721×10^{-25}	2.985×10^{19}	1.188×10^{21}	1.949×10^{21}	0.0251
$^{204}_{84}$Po	5.480	6.28	3.638×10^{-7}	1.376×10^{-26}	2.644×10^{19}	1.161×10^{21}	1.935×10^{21}	0.0228
$^{206}_{84}$Po	5.330	7.15	4.907×10^{-8}	2.254×10^{-27}	2.177×10^{19}	1.141×10^{21}	1.921×10^{21}	0.0191
$^{208}_{84}$Po	5.220	7.97	7.427×10^{-9}	5.727×10^{-28}	1.297×10^{19}	1.126×10^{21}	1.908×10^{21}	0.0115
$^{210}_{84}$Po	5.407	7.08	5.765×10^{-8}	7.615×10^{-27}	0.757×10^{19}	1.142×10^{21}	1.895×10^{21}	0.0065
$^{212}_{84}$Po	8.950	−6.52	2.295×10^{6}	4.598×10^{-14}	4.991×10^{19}	1.466×10^{21}	2.056×10^{21}	0.0341
$^{214}_{84}$Po	7.830	−3.87	5.138×10^{3}	4.309×10^{-17}	1.187×10^{20}	1.366×10^{21}	2.042×10^{21}	0.0873
$^{216}_{84}$Po	6.900	−0.82	4.580×10^{0}	3.670×10^{-20}	1.248×10^{20}	1.278×10^{21}	2.028×10^{21}	0.0976
$^{218}_{84}$Po	6.110	2.27	3.722×10^{-3}	2.844×10^{-23}	1.309×10^{20}	1.199×10^{21}	2.015×10^{21}	0.1092

to the oscillation frequency ω by

$$\nu_M = \frac{\omega}{2\pi} = \frac{\left(2n_r + \ell + \frac{3}{2}\right)\hbar}{2\pi\mu R_{\mathrm{n}}^2} = \frac{\left(G + \frac{3}{2}\right)\hbar}{1.2\pi\mu R^2}. \qquad (11)$$

The relationship $R_n^2 = \frac{3}{5}R^2$ is used. The global quantum number $G = 2n_r + \ell$ of a cluster state is estimated by the Wildermuth rule [23] as

$$G = 2n + \ell = \sum_{i=1}^{4} g_i, \qquad (12)$$

where n is the number of nodes of the α-core wave function, ℓ is the orbital angular momentum of the cluster motion, and g_i is the oscillator quantum number of a cluster nucleon. $g_i = 4$ for nuclei with $(Z, N) \leqslant 82$, $g_i = 5$ for $82 < (Z, N) \leqslant 126$, and $g_i = 6$ for $(Z, N) > 126$, corresponding to the $4\hbar\omega$, $5\hbar\omega$, and $6\hbar\omega$ oscillator shells, respectively, where N and Z are the proton and neutron numbers of the parent nucleus (see also Ref. [24]). However, since a heavy nucleus involves usually mixed oscillator shells, the determination of the G value with the Wildermuth rule can be ambiguous to some extent, usually with an uncertainty of 2 or 4 in even-even heavy nuclei [25].

The estimated microscopic assault frequency from Eq. (11) is shown in the eighth column of the Table I and Fig. 3 for even-even Po isotopes. The order of magnitude of ν_M is $10^{21}\ \mathrm{s}^{-1}$, the same as that of ν_C, which proves that the two calculations are consistent.

To study the correlation between the assault frequency and the structure properties, the values of $\nu/10^{21}\ \mathrm{s}^{-1}$ for the even-even Po isotopes used within the classical approach and estimated by the microscopic method are shown as a function of the neutron number in the Fig. 4 using triangles and black circles, respectively. The shapes of the two curves are similar, and the values of ν_M from the microscopic calculations are always larger than ν_C used classically but never beyond 2 times, implying again that the two different methods can be used. The assault frequency of the isotopes generally decreases with increasing neutron number up to the spherical shell closure $N = 126$, where the minimum of the assault frequency occurs, and then they increase quickly with the

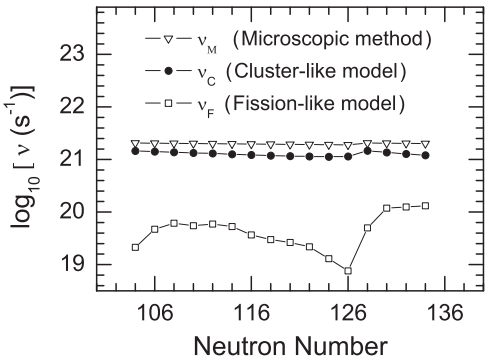

FIG. 3. $\log_{10}\nu$ for the even-even Po isotopes.

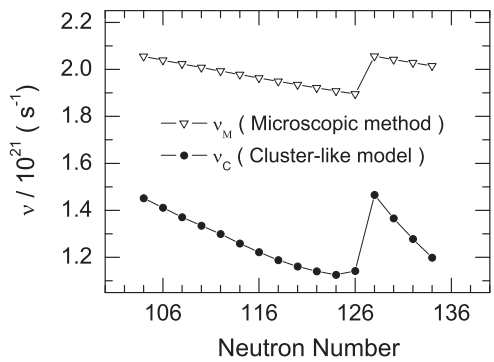

FIG. 4. $\nu/10^{21}$ for the even-even Po isotopes.

neutron number. It is clear that the α assault frequencies against the potential barrier are sensitive to the nuclear shell closure effects.

In conclusion, a study of the assault frequency and preformation factor of the α decay is performed from the experimental α-decay constant and the penetration probabilities calculated from the WKB approximation and the GLDM potential barriers. The approximation of a constant value of λ/P is relatively rough. To determine the assault frequency a quantum-mechanical method using a harmonic oscillator is introduced and leads to values of around 10^{21} s^{-1}, similar to the ones calculated within the classical method using the picture of a particle moving back and forth inside the nucleus. Then the preformation probability is around 10^{-1}–10^{-2}. The results for even-even Po isotopes from ground-state to ground-state α emissions are discussed for illustration. While the assault frequency presents only a shallow minimum in the vicinity of the magic neutron number 126, the preformation factor and mainly the penetrability probability diminish strongly around $N = 126$. The small value of the preformation factor suggests that the α decay is rather a radioactive emission process of a cluster formed on the surface of the nucleus but before the potential barrier penetration.

This work was supported by the National Natural Science Foundation of China (Grants No. 10775061, No. 10805061, and No. 10975064) and the CAS Knowledge Innovation Project No. KJCX-SYW-N02.

[1] G. Gamov, Z. Phys. **51**, 204 (1928).
[2] E. U. Condon and R. W. Gurney, Nature (London) **122**, 439 (1928).
[3] S. S. Malik and R. K. Gupta, Phys. Rev. C **39**, 1992 (1989).
[4] A. Ludu, A. Sandulescu, and W. Greiner, Int. J. Mod. Phys. E **1**, 169 (1992).
[5] C. Xu and Z. Z. Ren, Phys. Rev. C **74**, 014304 (2006).
[6] J. C. Pei, F. R. Xu, Z. J. Lin, and E. G. Zhao, Phys. Rev. C **76**, 044326 (2007).
[7] G. L. Zhang, X. Y. Le, and H. Q. Zhang, Nucl. Phys. A **823**, 16 (2009).
[8] T. Dong and Z. Ren, Phys. Rev. C **82**, 034320 (2010).
[9] D. N. Poenaru, M. Ivascu, A. Sandulescu, and W. Greiner, Phys. Rev. C **32**, 572 (1985); D. N. Poenaru, I. H. Plonski, and W. Greiner, *ibid.* **74**, 014312 (2006).
[10] G. Royer, J. Phys. G **26**, 1149 (2000).
[11] P. R. Chowdhury, D. N. Basu, and C. Samanta, Phys. Rev. C **75**, 047306 (2007).
[12] V. Yu. Denisov and A. A. Khudenko, At. Data Nucl. Data Tables **95**, 815 (2009).
[13] G. Royer and H. F. Zhang, Phys. Rev. C **77**, 037602 (2008).
[14] G. Royer, Nucl. Phys. A **848**, 279 (2010).
[15] H. F. Zhang, W. Zuo, J. Q. Li, and G. Royer, Phys. Rev. C **74**, 017304 (2006).
[16] H. F. Zhang and G. Royer, Phys. Rev. C **77**, 054318 (2008).
[17] G. Royer and B. Remaud, Nucl. Phys. A **444**, 477 (1985).
[18] Y. Z. Wang, H. F. Zhang, J. M. Dong, and G. Royer, Phys. Rev. C **79**, 014316 (2009).
[19] G. Audi, O. Bersillon, J. Blachot, and A. H. Wapstra, Nucl. Phys. A **729**, 3 (2003).
[20] J. Dvorak *et al.*, Phys. Rev. Lett. **97**, 242501 (2006).
[21] S. Hofmann and G. Münzenberg, Rev. Mod. Phys. **72**, 733 (2000); S. Hofmann *et al.*, Eur. Phys. J. A **32**, 251 (2007).
[22] Yu. Ts. Oganessian *et al.*, Phys. Rev. C **63**, 011301(R) (2000); **70**, 064609 (2004); **72**, 034611 (2005); **74**, 044602 (2006); **76**, 011601(R) (2007).
[23] K. Wildermuth and Y. C. Tang, *A Unified Theory of the Nucleus* (Academic, New York, 1977).
[24] P. Mohr, Phys. Rev. C **61**, 045802 (2000).
[25] B. Buck, A. C. Merchant, and S. M. Perez, Phys. Rev. C **51**, 559 (1995).